*photonics*

MDPI

*Article*

# Reconfigurable Photonic Integrated Circuits in Glass by Femtosecond Laser Writing and Laser-Induced Chemical Etching

**Philip Lichtenegger *, Philipp Hurdax, Georg Spernbauer and Bernhard Lamprecht**

MATERIALS—Institute for Sensors, Photonics and Manufacturing Technologies, JOANNEUM RESEARCH Forschungsgesellschaft mbH, Franz-Pichler-Straße 30, 8160 Weiz, Austria
* Correspondence: philip.lichtenegger@joanneum.at

**Abstract**

Femtosecond laser writing (FLW) enables mask-free three-dimensional photonic integration in transparent materials and offers a flexible route for prototyping glass-based photonic circuits. Here, we present a monolithic fabrication approach that combines femtosecond laser waveguide writing, femtosecond laser-induced chemical etching (FLICE), laser ablation, and metallization to realize reconfigurable photonic circuits in borosilicate glass. The process is implemented in a CAD-to-device workflow that allows optical, mechanical, and electrical structures to be co-designed and fabricated within the same substrate. A stress-assisted waveguide-writing regime is developed in borosilicate glass, enabling single-scan fabrication of optical waveguides, directional couplers, and Mach–Zehnder interferometers at writing speeds of 30 mm/s. The fabricated devices demonstrate stable guiding, directional coupling, and interferometric operation, providing a practical basis for implementing reconfigurable photonic building blocks in this material platform. FLICE is then used to fabricate suspended glass microbridges incorporating femtosecond-laser-written waveguides and integrated resistive microheaters. These structures act as thermally isolated thermo-optic phase shifters and enable a full $2\pi$ phase shift with an electrical power consumption of approximately 17 mW. The results demonstrate the feasibility of combining FLW and FLICE within a single borosilicate glass substrate to monolithically integrate passive photonic circuits with actively tunable thermo-optic phase shifters. This work establishes a laser-based fabrication route for reconfigurable three-dimensional photonic circuits in glass and provides a basis for future optimization toward larger programmable photonic systems.

**Keywords:** femtosecond laser writing; femtosecond laser-induced chemical etching; selective laser-induced etching; borosilicate glass; integrated photonics; optical waveguides; thermo-optic phase shifters; reconfigurable photonic circuits

Check for updates

Received: 1 July 2026
Revised: 27 July 2026
Accepted: 28 July 2026
Published: 31 July 2026

**Copyright:** © 2026 by the authors. Licensee MDPI, Basel, Switzerland. This article is an open access article distributed under the terms and conditions of the Creative Commons Attribution (CC BY) license.

## 1. Introduction

Programmable photonic integrated circuits provide a versatile platform for implementing reconfigurable linear optical transformations on a chip. By combining waveguides, directional couplers, interferometers, and phase-control elements, such circuits enable controlled splitting, recombination, and phase manipulation of optical fields within compact and phase-stable architectures. They are relevant across classical and quantum photonics, including optical signal processing, precision sensing, and quantum information processing, where programmable interference and scalable optical connectivity are key requirements [1–4]. In particular, interferometric meshes based on tunable Mach–Zehnder

interferometers (MZIs) provide a general architecture for realizing programmable linear optical transformations and have become a key building block for universal multiport interferometers and photonic processors [5,6].

Dynamic reconfiguration in integrated photonic circuits is commonly achieved by locally controlling the optical phase. Thermo-optic phase shifters are attractive in this context because they are conceptually simple, compatible with many material platforms, and can be integrated using resistive microheaters placed close to optical waveguides [7–9]. However, thermo-optic tuning also introduces important design constraints. The dissipated heat must be efficiently delivered to the target phase-shifting region in order to reduce electrical power consumption and to limit unwanted thermal coupling to neighbouring components [9–11]. These requirements become increasingly important as photonic circuits scale from individual interferometers to larger programmable meshes.

Planar lithographic photonic platforms have enabled high-density integration and wafer-scale manufacturing. Their largely two-dimensional fabrication geometry, however, can restrict design freedom for intrinsically three-dimensional optical architectures. Femtosecond laser writing offers a complementary fabrication route. By focusing ultrashort laser pulses inside transparent substrates, permanent refractive index modifications can be produced locally, allowing optical waveguides and three-dimensional photonic circuits to be written directly in the bulk of glass or other dielectric materials [12–14]. Because this process is mask-free and compatible with rapid design iteration, it is particularly attractive for prototyping, small-batch device development, and photonic architectures that benefit from three-dimensional routing. The principle of femtosecond laser writing in glass is illustrated in Figure 1.

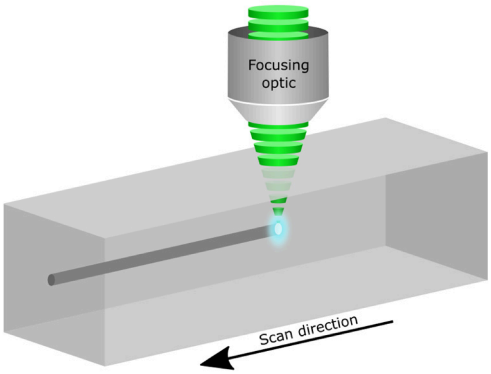


**Figure 1.** Principle of FLW in glass. Nonlinear absorption of tightly focused ultrashort laser pulses generates a localized electron plasma within the transparent substrate. Rapid energy transfer from the plasma to the lattice induces permanent structural modifications [15]. By translating the substrate relative to the laser focus, continuous three-dimensional structures can be inscribed with micrometer-scale precision.

Femtosecond-laser-written photonic circuits have matured substantially over the past two decades and now support a broad range of passive and reconfigurable glass-based photonic devices. Low-loss waveguides, directional couplers, interferometers, multiport circuits, and three-dimensional quantum photonic networks have been demonstrated in several glass platforms [8,12,13,16–18]. Multiscan writing strategies and mode-field engineering have further improved waveguide performance by enabling tailored refractive index profiles, improved mode matching, and propagation losses below 0.1 dB/cm in optimized fused silica platforms [19]. In parallel, reconfigurable laser-written glass circuits incorporating thermo-optic phase shifters have demonstrated programmable multiport interferometers and, more recently, FLW-based universal photonic processors, confirming the potential of FLW for reconfigurable photonics [20–23].

In FLW-based glass circuits, thermo-optic tuning is typically implemented by depositing or patterning resistive heaters near laser-written waveguides. The efficiency of such phase shifters can be improved by thermally isolating the heated waveguide section from the surrounding substrate. Previous work has shown that thermal isolation structures can reduce the power required for thermo-optic phase tuning in laser-written photonic circuits and can support more compact reconfigurable layouts [9,10,21]. Nevertheless, further integration strategies are of interest for combining optical waveguides, electrical heaters, and mechanically defined thermal isolation structures in a monolithic and reproducible fabrication workflow.

Femtosecond laser-induced chemical etching (FLICE), also known as selective laser-induced etching (SLE), extends FLW by enabling the selective removal of laser-modified material through wet-chemical etching. This process enables the fabrication of buried channels, suspended structures, and complex three-dimensional microdevices directly within transparent glass substrates [24–26]. FLICE has been widely applied to glass microfluidics and optofluidics, including the monolithic integration of laser-written optical waveguides with microfluidic channels and other three-dimensional microstructures [27–30]. These capabilities make FLICE an attractive technique for extending FLW-based photonic circuits with mechanically defined thermal isolation structures and other integrated microcomponents.

In this work, we demonstrate a laser-based fabrication route for reconfigurable photonic circuits in borosilicate glass by combining FLW and FLICE within a single substrate. The central device concept is a suspended glass microbridge that carries both a femtosecond-laser-written optical waveguide and an integrated resistive microheater, thereby forming a thermally isolated thermo-optic phase shifter inside a Mach–Zehnder interferometer. The aim of this study is to establish the feasibility of this monolithic integration approach and to validate the basic photonic and thermo-optic functionality of the resulting devices.

The fabrication platform is first assessed through waveguide, directional coupler, and interferometer structures written in SCHOTT BOROFLOAT® 33 borosilicate glass (BF33) using a single-scan stress-assisted writing regime. This regime enables the fabrication of optical waveguides and interferometric building blocks at writing speeds of 30 mm/s. Subsequently, FLICE-fabricated suspended microbridges are integrated with interferometric circuits and metallized microheaters to demonstrate active phase tuning. The resulting thermo-optic phase shifters achieve a full $2\pi$ phase shift with an electrical power consumption of approximately 17 mW.

The novelty of the present work lies in the monolithic integration of femtosecond-laser-written photonic building blocks with FLICE-fabricated suspended thermo-optic tuning structures in borosilicate glass. While reconfigurable FLW photonic circuits and FLICE-based glass microstructures have been demonstrated previously, the combination of a laser-written waveguide and a resistive microheater on a suspended FLICE-fabricated microbridge provides a distinct route toward thermally isolated active tuning in glass-based photonic circuits. This study serves as a proof-of-principle demonstration of the fabrication concept and device functionality, providing a foundation for future work on statistical process characterization, thermal crosstalk analysis, long-term stability, and scaling toward larger programmable photonic circuits.

## 2. Materials and Methods

**Experimental FLW Setup:** Femtosecond laser processing was performed using the frequency-doubled output (524 nm) of a Spectra-Physics Spirit laser system. The use of the second harmonic was selected to reduce the diffraction-limited focal volume compared with the fundamental wavelength and to provide improved spatial resolution during volume modification and surface ablation. The laser system allowed adjustment of the

pulse duration between 209 fs and 10 ps and operation at repetition rates from single-shot mode up to 1 MHz. Unless stated otherwise, pulse energies reported in this work were calculated from the average laser power measured after the focusing optic and the applied repetition rate.

The average laser power was controlled by a combination of a half-wave plate and a polarizing beam splitter. In addition, the internal voltage-controlled attenuator of the laser system was used for dynamic power modulation during synchronized motion. The beam diameter was adjusted with a beam expander to match the entrance aperture of the focusing optics. The polarization state of the writing beam could be selected as either linear or circular. Circular polarization was used for both waveguide writing and FLICE exposure.

The substrate was positioned in the XY plane using motorized translation stages (XML210-S; Newport Corporation, Irvine, CA, USA), while the focusing and imaging optics provided Z positioning via a motorized linear stage (IMS100V; Newport Corporation, Irvine, CA, USA). All motion axes were controlled by an XPS-D motion controller (Newport Corporation, Irvine, CA, USA). The controller was operated in Point–Velocity–Time (PVT) mode for synchronized multi-axis trajectories. Each trajectory segment was defined by its displacement, target velocity, and execution time, and smooth interpolation between points was applied to avoid discontinuities in writing speed. Analog outputs of the motion controller were used to synchronize the laser power modulation with the programmed writing trajectory.

Three-dimensional writing trajectories were generated via custom Python scripts (Python 3.9.10; Python Software Foundation, Wilmington, DE, USA) implemented within the Rhinoceros 3D CAD environment (Rhinoceros 8; Robert McNeel & Associates, Seattle, WA, USA). The scripts defined the geometric path of the structures and associated process parameters, including writing speed and analog control signals for laser-power adjustment. The resulting motion programs were transferred to the motion controller and executed under computer control. This workflow enabled the direct fabrication of three-dimensional photonic and microstructural elements from CAD-defined layouts.

A schematic of the optical setup is shown in Figure 2. The laser beam was focused into the transparent substrate at depths between approximately 200 µm and 500 µm below the sample surface. An inline microscope was used for sample alignment, focusing, and in situ process monitoring. Two non-polarizing 50:50 beamsplitters were incorporated into the setup. The first beamsplitter enabled coaxial imaging of the substrate and laser focus, while the second beamsplitter enabled monitoring of the transmitted processing beam. This monitoring path was used to observe beam-pointing stability and relative power stability during processing.

Different focusing optics were used for the individual fabrication steps. The setup accommodated microscope objectives with numerical apertures (NA) between 0.13 and 0.55 for alignment marking, FLICE exposure, scribing, and metal patterning. Waveguide writing was performed with an aspheric lens with a numerical aperture of 0.55. Unless stated otherwise, all BF33 waveguides reported in this work were fabricated using this lens. To tailor the focal volume for stress-assisted waveguide formation in BF33, a 400 µm-thick borosilicate glass plate was attached directly to the aspheric lens to introduce controlled spherical aberration. This configuration was used as a fixed process condition for the BF33 waveguide-writing experiments. The writing depth was chosen such that the resulting modification geometry supported stable stress-assisted guiding.

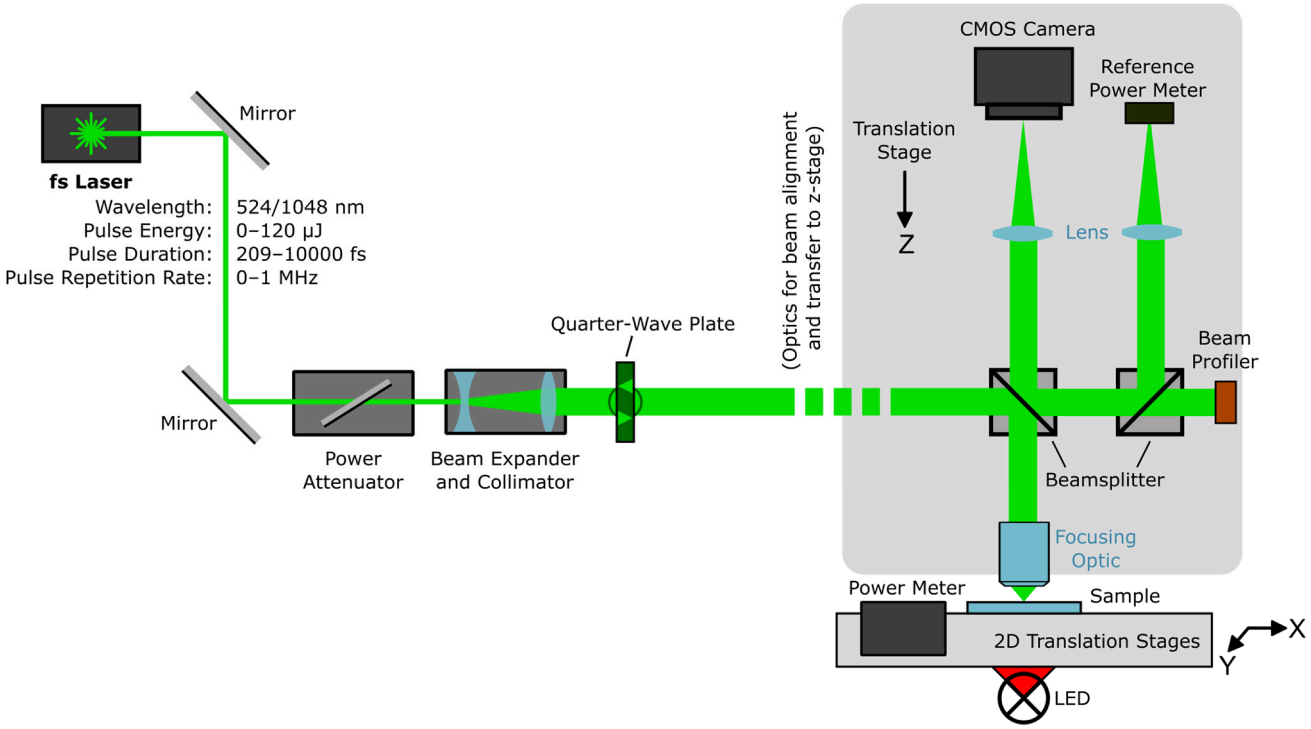


**Figure 2.** Schematic of the femtosecond laser writing setup for waveguide fabrication and laser-based microstructuring. The frequency-doubled output of the femtosecond laser system is expanded and focused into the transparent substrate. Beam splitters provide coaxial imaging and process monitoring. Three-dimensional structures are fabricated by synchronized motion of the sample stages and focusing optics under computer control.

**Substrate Materials:** Experiments were performed with BF33 borosilicate glass and high-purity fused silica substrates. Both materials are transparent in the visible and near-infrared spectral range and are compatible with femtosecond laser processing. Fused silica was primarily used to validate established multiscan waveguide-writing and FLICE procedures, whereas BF33 borosilicate glass served as the main substrate material for the reconfigurable photonic circuits demonstrated in this work.

The substrates had lateral dimensions of up to 20 × 50 $mm^2$ and thicknesses between 400 µm and 1.1 mm. Prior to laser processing, the substrates were cleaned by sequential rinsing with acetone and isopropanol, followed by drying with compressed air. For processing steps requiring high positional accuracy, laser-ablated alignment marks were written onto the substrate surface, which served as reference features for subsequent waveguide writing, FLICE exposure and metal patterning.

**Femtosecond Laser-Induced Modification Regimes in Glass:** Femtosecond laser irradiation of transparent dielectrics can induce different types of permanent material modification depending on the deposited energy density, pulse duration, repetition rate, focusing conditions, translation speed, and glass composition [15]. At relatively low deposited energy densities, smooth refractive index changes can be generated. These so-called Type-I modifications are commonly used for low-loss optical waveguides, particularly in fused silica, where the laser-exposed region can exhibit a positive refractive index change.

At higher deposited energy densities, the modification regime transitions to so-called Type-II modifications, which are characterized by anisotropic structures, nanograting formation, birefringence, crack-like morphologies, and, in some materials, enhanced chemical reactivity. These modification regimes are relevant for femtosecond laser-induced chemical etching, because the laser-exposed regions can exhibit substantially higher etch rates than

the unmodified glass. The dominant microscopic mechanism depends on the material and irradiation conditions and is therefore not assumed to be identical for fused silica and BF33.

At still higher pulse energies, laser exposure can lead to void formation, micro-explosions, or surface ablation. These modifications generally introduce excessive optical scattering and are not suitable for low-loss waveguide cores. In the present work, however, ablation was intentionally used for auxiliary fabrication steps such as alignment marks, substrate scribing, and metal patterning.

The waveguide formation mechanisms in fused silica and BF33 differ substantially, as illustrated in Figure 3. In fused silica, guiding is based on Type-I refractive index modification [12]. The optical mode is located within the laser-written region. To tailor the waveguide cross-section and mode-field geometry, a multiscan writing strategy consisting of 21 laterally shifted scans with a pitch of 0.25 µm was employed, resulting in a nearly square waveguide cross-section [19].

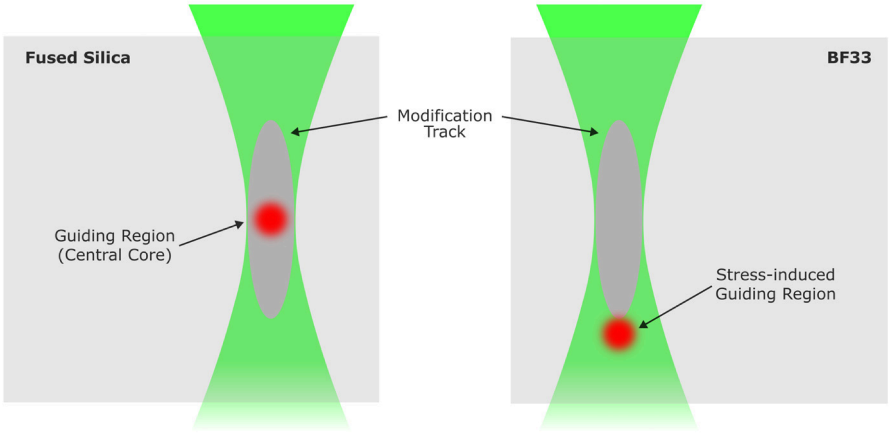


**Figure 3.** Schematic illustration of waveguide formation in fused silica and BF33 borosilicate glass. In fused silica, guiding occurs within the laser-written Type-I modification. In BF33, the optical mode is formed in a stress-assisted guiding region displaced from the central laser-modified track. For the process conditions used in this work, guiding was observed predominantly below the written track.

In BF33, the waveguides investigated in this work were formed in a stress-assisted writing regime [31,32]. Under the selected process conditions, the central laser-modified region did not act as the optical core. Instead, optical guiding occurred in a neighboring region whose refractive index was increased by laser-induced residual stress. The relative displacement between the central modification track and the stress-assisted guiding region was taken into account when designing waveguide arrays, directional couplers, and Mach–Zehnder interferometers. For the process parameters used in this work, the guiding region was consistently located approximately 10 µm below the central modification track.

This stress-assisted writing regime enabled reproducible single-scan fabrication of waveguides in BF33 at a writing speed of 30 mm/s and was employed for all BF33 waveguides, directional couplers, and Mach–Zehnder interferometers presented in this work. In contrast, the fused silica reference structures used for platform validation were fabricated using a multiscan approach [19].

**Femtosecond Laser-Induced Chemical Etching (FLICE)** was used to fabricate three-dimensional microstructures inside the glass substrates. The process comprises two steps. First, regions to be removed were exposed to focused ultrashort laser pulses. Second, the samples were immersed in an alkaline etchant to selectively remove the laser-modified material.

For FLICE exposure, the laser parameters were chosen to generate modifications with enhanced etchability rather than optical guiding. The process parameters used for fused silica and BF33 are summarized in Table 1. For both BF33 and fused silica, FLICE structures

were written using a 20× objective (NA = 0.5). Depending on the geometry of the structure, scan speeds between 1 and 10 mm/s were employed. Hatch distances of 2–6 µm were used, while the slicing distance was kept constant at 4 µm. All FLICE exposures were performed using circular polarization. For suspended microbridge structures, the FLICE volume was designed to define the air gaps surrounding the waveguide-carrying microbridge. Several bridge geometries were investigated, including suspended microbridges and designs incorporating through-substrate FLICE structures. The latter were fabricated as a proof-of-principle for future thermally managed device architectures in which the microbridge could be coupled to an external heat sink. The thermal performance of these structures was not investigated in the present work. The microbridges were aligned to previously written waveguides using laser-ablated surface alignment marks, which were registered through the inline microscope of the writing system. The alignment procedure was validated by the successful fabrication and optical inspection of dedicated waveguide–microbridge alignment test structures.

**Table 1.** Summary of nominal laser processing parameters used for the different fabrication steps in fused silica (FS) and borosilicate glass (BF33).

| Process Step | Pulse Duration (fs) | Repetition Rate (kHz) | Pulse Energy (µJ) | Scan Speed (mm/s) | Overscans | Focusing Optics |
|---|---|---|---|---|---|---|
| Scribe and Break | 209 | 125 | 10.56 | 3 | 6 | 10× objective (NA 0.25) |
| Alignment Marks (FS) | 1000 | 125 | 0.2 | 2 | 3 | 10× objective (NA 0.25) |
| Alignment Marks (BF33) | 2500 | 25 | 1.5 | 2 | 1 | 10× objective (NA 0.25) |
| Waveguide Writing (FS) | 209 | 1 | 0.036 | 1 | 21 | Asphere (NA 0.55) |
| Waveguide Writing (BF33) | 209 | 1 | 0.12 | 30 | 1 | Asphere (NA 0.55) |
| FLICE Writing (FS) | 1000 | 125 | 0.2 | 1–10 | 1 | 20× objective (NA 0.5) |
| FLICE Writing (BF33) | 2500 | 25 | 0.5 | 1–10 | 1 | 20× objective (NA 0.5) |
| Metal Patterning | 209 | 1 | 0.55 | 2 | 3 | 5× objective (NA 0.13) |

After laser exposure, the samples were etched overnight in 8 M KOH at 80 °C under continuous ultrasonic agitation, corresponding to a typical etching time of approximately 16 h. The exact etching duration was not found to be critical within this process window, provided that the laser-modified sacrificial regions were removed completely. Ultrasonic agitation supported etchant transport into the laser-modified regions and removal of reaction products. After etching, the samples were rinsed thoroughly in deionized water and dried with compressed air. The resulting suspended microbridges were inspected by optical microscopy to verify complete release and mechanical integrity.

**Femtosecond Laser Ablation** was used for three auxiliary fabrication steps. First, alignment marks were ablated on the substrate surface to provide reference features for successive processing steps. Second, shallow ablation grooves were written to define scribe lines for controlled cleaving of the glass chips. Third, after metal deposition, selective ablation of the metallic layer was used to define electrically isolated heater and contact structures.

For substrate scribing, ablation lines were written employing a 10× objective with a numerical aperture of 0.25. The samples were subsequently cleaved along the scribe lines. For metal patterning, the Cr/Au layer was locally removed using a 5× objective with a numerical aperture of 0.13. The metal patterning parameters were optimized to remove the conductive film while minimizing damage to the underlying glass substrate. The electrical isolation of the patterned metal structures was verified by resistance measurements between adjacent contact pads.

**Photonic Chip Fabrication Workflow:** The fabrication workflow combined waveguide writing, FLICE microstructuring, selective chemical etching, facet preparation, metalliza-

tion, metal patterning, and chip mounting and electrical interfacing. The individual process steps are summarized schematically in Figure 4.

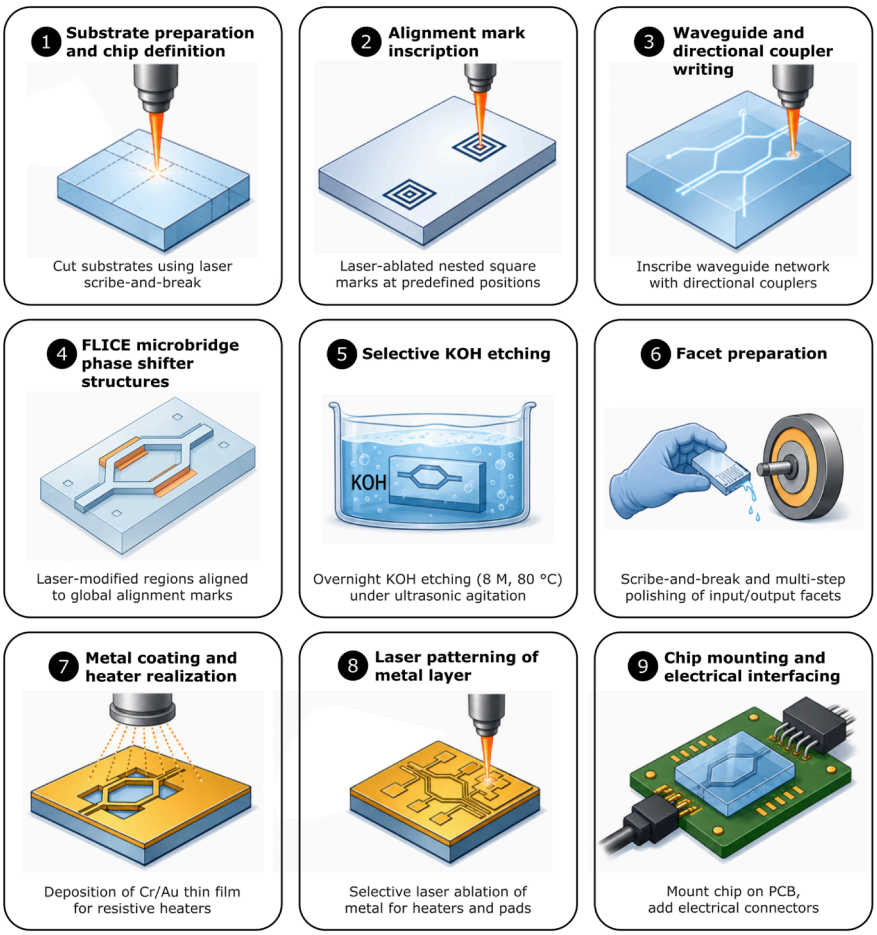


**Figure 4.** Schematic overview of the laser-based fabrication workflow for integrated photonic chips. The process includes: (1) substrate preparation by scribe-and-break, (2) laser-ablated alignment marks, (3) waveguide and directional coupler inscription, (4) FLICE exposure of suspended microbridge structures, (5) selective KOH etching, (6) facet preparation by cleaving and polishing, (7) Cr/Au metallization, (8) laser patterning of electrical contacts and heater structures, and (9) chip mounting on a printed circuit board. The figure is intended as a conceptual process illustration and is not drawn to scale, nor does it represent the exact final MZI geometry. Device dimensions and heater position are described in detail in the text.

Fabrication started with substrate preparation by femtosecond laser scribing and controlled cleaving to the desired chip dimensions. Laser-ablated alignment marks were then written onto the substrate surface. These marks served as reference features for the registration of waveguide, FLICE, and metallization patterns.

Next, the optical waveguide network was written into the glass substrate. For BF33 devices, a single-scan stress-assisted writing process was used. The written photonic structures included straight waveguides, directional couplers, and Mach–Zehnder interferometers for optical and thermo-optic characterization. For validation experiments in fused silica, multiscan waveguides were written using the parameters listed in Table 1.

After waveguide writing, the FLICE patterns for the suspended microbridges were written. The bridge structures were positioned in one arm of selected Mach–Zehnder interferometers. The FLICE exposure was aligned to the waveguide layout using the previously written alignment marks. After exposure, the samples were etched in KOH to remove the modified sacrificial volumes and expose the suspended glass microbridges.

Following FLICE processing, the chips were trimmed to their final dimensions. The input and output facets were prepared by scribing, cleaving and mechanical polishing. A Cr/Au bilayer with nominal thicknesses of 2 nm and 50 nm, respectively, was deposited by thermal evaporation over the entire chip surface. The metal layer served both as the resistive heater material and as the contact metallization. Electrical isolation trenches and contact pads were subsequently defined by femtosecond laser ablation of the metal film. The heater was positioned on the top surface of the suspended microbridge above the waveguide-carrying MZI arm. In the present implementation, the heater layout followed the CAD geometry of the FLICE-fabricated suspended bridge. For the devices demonstrated in this work, a fixed bridge geometry with a nominal cross-section of 60 µm × 60 µm and a length of 3 mm was selected, with the resistive heater extending along the waveguide-carrying microbridge section. After metal patterning, the nominal electrical resistance of the heater was approximately 50 Ω. Finally, the chips were mounted on custom printed circuit boards using conductive adhesive for electrical contacts and structural adhesive for mechanical stabilization.

The laser-processing parameters used for the individual fabrication steps are summarized in Table 1. Pulse energies were calculated from the average power measured after the focusing optic and the applied repetition rate. The listed values represent the nominal process parameters used for the devices reported in this work.

**Optical Characterization:** The fabricated waveguides and interferometric devices were characterized by optical microscopy, near-field mode imaging, transmission measurements, and thermo-optic tuning measurements. Initial inspection of the chip surface and cleaved facets was performed using optical microscopy to verify waveguide continuity, facet quality, and the integrity of the suspended microbridge structures.

Continuous-wave laser sources at 633 nm and 808 nm were used for optical characterization. The devices were designed for operation at 808 nm, which was used as the primary characterization wavelength. The directional coupler and MZI geometries were therefore optimized experimentally for operation at 808 nm. While the laser-written waveguides may guide over a broader spectral range, the directional coupler splitting ratio and interferometer response are wavelength dependent. Broadband operation was not systematically investigated in this work. In addition, a 633 nm source was employed as a visible auxiliary wavelength for alignment, inspection, and preliminary stability checks. Light was coupled into the waveguides by end-fire coupling by means of a microscope objective with NA = 0.1 mounted on a three-axis NanoMax stage. The chip was positioned on a three-axis micrometer stage. The input polarization was controlled using a polarizer and a quarter-wave plate. Coarse alignment was performed with an overhead microscope, followed by fine alignment based on maximization of the transmitted optical power.

The output mode profile was imaged from the output facet onto a CMOS camera using a 20× microscope objective with NA = 0.4. The recorded near-field intensity distributions were analyzed to determine the mode-field diameter employing the D4σ method. Optical transmission was measured using a calibrated optical power meter. The reported transmission values were calculated from the ratio of output power to input power. They therefore correspond to total insertion loss rather than pure propagation loss and include propagation loss, input and output coupling losses, Fresnel reflections, facet-related losses, and additional losses caused by waveguide imperfections. The pure propagation loss was extracted separately by cut-back analysis on waveguides with different lengths. The optical and thermo-optic characterization setup is shown schematically in Figure 5.

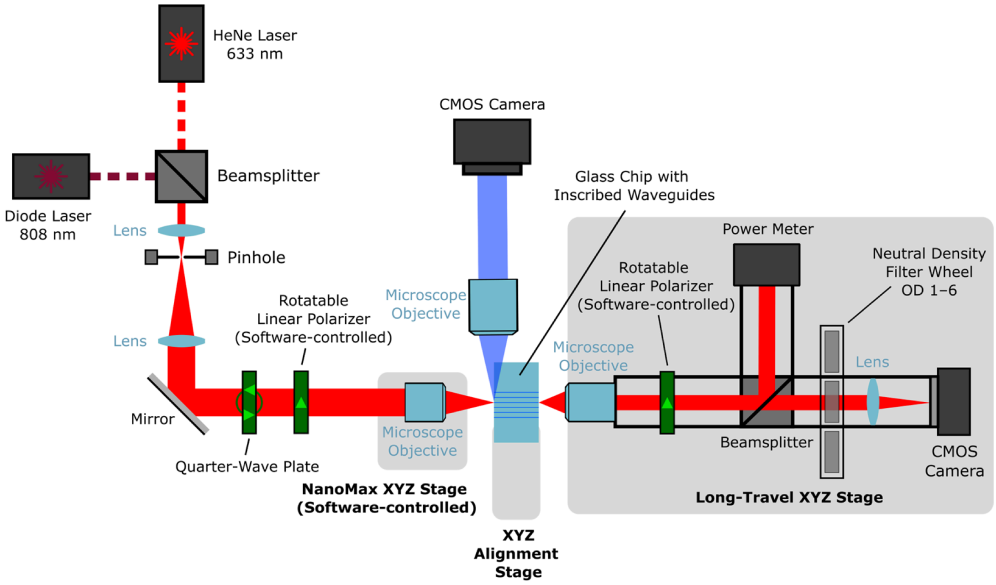


**Figure 5.** Schematic of the optical and thermo-optic characterization setup. The setup enables end-fire coupling, polarization control, near-field mode imaging, transmission measurements, and characterization of thermo-optic phase shifters integrated into Mach–Zehnder interferometers.

Thermo-optic phase shifters were characterized by electrically actuating the resistive heaters integrated into one arm of a Mach–Zehnder interferometer while monitoring the optical transmission. A Keithley 2401 SourceMeter (Keithley Instruments, Cleveland, OH, USA), controlled by a LabVIEW program (LabVIEW 2023 Q1; National Instruments, Austin, TX, USA), was used to generate voltage ramps and record the applied voltage, current, and transmitted optical power. During characterization, light was coupled into one input waveguide of the MZI, and the output power at the bar and cross-ports was recorded as the electrical heater power was increased. The electrical power dissipated in the resistive heater required to induce a $2\pi$ phase shift was determined from one complete period of the MZI transmission response.

These measurements validated active phase tuning of the suspended microbridge structures. Quantitative thermal crosstalk between neighboring phase shifters was not measured in this study and remains the subject of future work.

## 3. Results

**Multiscan Waveguides in Fused Silica:** As a first step toward establishing the femtosecond laser fabrication workflow, multiscan waveguides were fabricated in fused silica using a writing strategy based on laterally shifted Type-I modifications. This approach has previously been shown to enable nearly square refractive index profiles, improved mode matching to standard single-mode fibers, and propagation losses among the lowest reported for femtosecond-laser-written waveguides in fused silica [19]. In the present work, these structures served primarily as a reference process for validating the fabrication workflow and benchmarking the experimental setup.

To identify a suitable Type-I writing regime, single-scan waveguides were first inscribed at a depth of 400 µm while varying the pulse energy. A transition from smooth Type-I modifications to modifications with Type-II-like features was observed at pulse energies of approximately 36 nJ. Below this value, the laser-written tracks showed smooth morphology and supported optical guiding, whereas higher pulse energies resulted in structural features that were not suitable for low-loss waveguide fabrication.

Based on these observations, multiscan waveguides were fabricated using pulse energies close to, but below, the observed Type-II transition. A 21-scan multiscan pattern

with a lateral pitch of 0.25 µm produced a nearly square waveguide cross-section. Laser writing was performed at a wavelength of 524 nm using 209 fs pulses, a repetition rate of 1 MHz, and circular polarization. The beam was focused 400 µm below the sample surface using the NA = 0.55 aspheric lens and the focal-volume shaping configuration described in Section 2. The resulting structures exhibited homogeneous, nearly square cross-sections, confirming successful implementation of the multiscan writing approach within the developed fabrication platform (Figure 6).

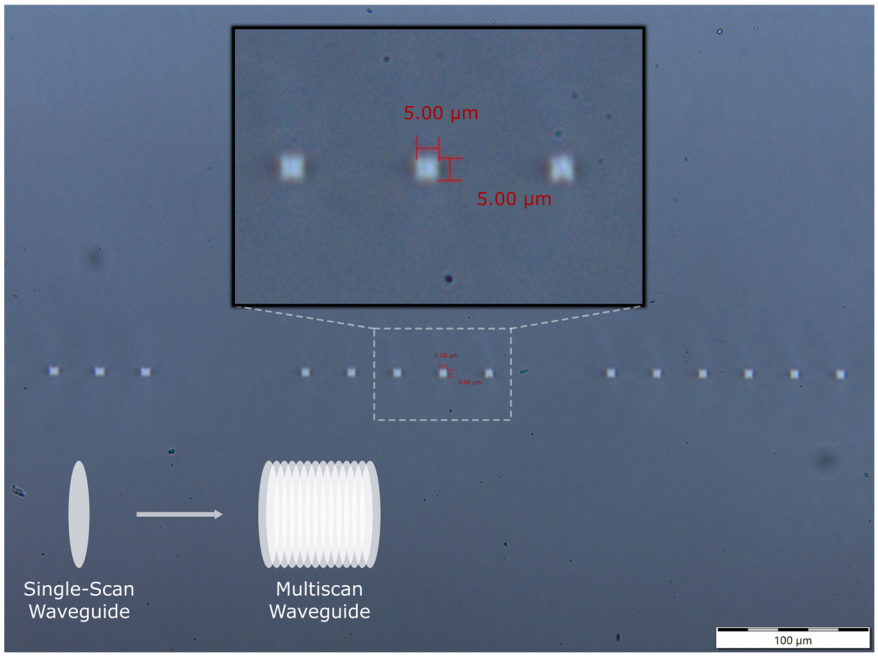


**Figure 6.** Facet-view optical transmission micrographs of fused silica waveguides fabricated with the multiscan approach. The structures exhibit a nearly square cross-section formed by multiple adjacent Type-I modifications. The inset schematically illustrates the fabrication strategy, including identification of the Type-I writing regime and subsequent multiscan waveguide fabrication.

Although the characteristic morphology and guiding behavior of the multiscan waveguides reported by Skryabin et al. could be successfully reproduced, the measured propagation loss of approximately 0.3 dB/cm remained above the state-of-the-art value of 0.07 dB/cm reported for optimized multiscan waveguides in fused silica [19]. This difference is attributed primarily to the demanding stability requirements of the multiscan process, which involves long writing times and repeated scans with submicrometer lateral offsets. The fused silica multiscan experiments therefore served as a useful benchmark for validating the fabrication workflow, but they also motivated the investigation of an alternative glass platform enabling faster single-scan waveguide fabrication.

**Stress-Assisted Waveguides in BF33 Glass:** The following results focus on stress-assisted waveguides fabricated in BF33 borosilicate glass, which form the basis of the reconfigurable photonic circuits demonstrated in this work. A single-scan writing strategy at translation speeds of several tens of millimetres per second was chosen to minimize fabrication time and reduce the sensitivity to slow process drifts during the writing of complex circuits. Under the selected writing conditions—524 nm wavelength, 209 fs pulse duration, 1 MHz repetition rate, circular polarization, 200 µm writing depth, single-scan writing, and an NA = 0.55 aspheric lens combined with a 400 µm glass plate for focal-volume shaping—optical waveguides were obtained over a comparatively broad range of pulse energies and writing speeds.

In contrast to the Type-I guiding observed in fused silica, optical guiding in BF33 occurred in a region spatially displaced from the central laser-modified zone. Transmission microscopy of the waveguide cross-sections revealed an elongated modification track, while the guided optical mode was located in a separate region below this track. For the process conditions used in this work, the displacement between the central modification and the guiding region was approximately 10 µm. This behavior is consistent with stress-assisted guiding mechanisms reported for borosilicate and other multicomponent glasses, where laser-induced material modification and the associated stress field can generate a guiding region outside the directly modified zone [31,32].

Figure 7 shows waveguides fabricated across the investigated parameter range of pulse energy and writing speed. Across a wide range of pulse energies and writing speeds, the characteristic morphology remained essentially unchanged: the laser-modified region was consistently separated from the optical guiding region by approximately 10 µm. This indicates that the underlying stress-assisted waveguide formation mechanism is robust over a broad processing window and exhibits low sensitivity to moderate variations in the investigated laser parameters. Such robustness is particularly advantageous for practical device fabrication, where small fluctuations in pulse energy, focusing conditions, or other process parameters cannot be entirely avoided.

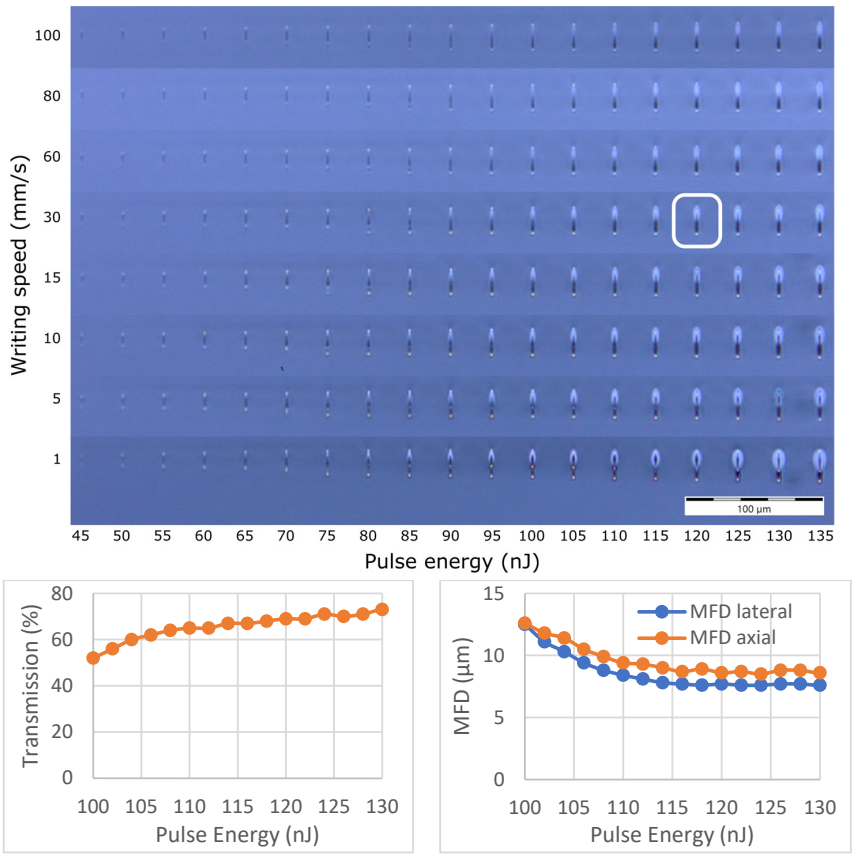


**Figure 7.** Stress-assisted waveguide fabrication in BF33. (**Top**) facet-view optical transmission micrographs of waveguides fabricated over a range of pulse energies and writing speeds. A characteristic separation between the central laser-modified track and the optical guiding region is observed for a broad portion of the investigated parameter space. The white frame highlights the parameter set selected for further device fabrication. (**Bottom left**) measured transmission as a function of pulse energy for waveguides fabricated at a writing speed of 30 mm/s. (**Bottom right**) corresponding mode-field diameter as a function of pulse energy. The inset shows a representative near-field profile of the guided fundamental mode. The plotted transmission and mode-field diameter values are representative measurements used to identify a suitable process window.

Based on the parameter study, a writing speed of 30 mm/s was selected for subsequent device fabrication because it combined high fabrication throughput with stable waveguide properties. At this writing speed, both the transmission and, more importantly, the mode-field diameter remained essentially constant within the experimental uncertainty over a pulse-energy interval of approximately ±10 nJ around the selected pulse energy of 120 nJ. This behavior contrasts with the fused silica multiscan process implemented in this work, where small pulse-energy changes produced more pronounced variations in transmission and mode-field properties.

In this stress-assisted regime, the optical mode is not located inside the central laser-modified track but in the adjacent stress-modified region. Therefore, a moderate increase in pulse energy can improve the stress-induced guiding and mode confinement without necessarily causing an immediate decrease in transmission due to defects in the directly modified voxel. The transmission trend in Figure 7 should therefore be interpreted as a process-window characterization rather than as a statistically complete optimization curve.

The selected pulse energy should be understood as a robust practical writing condition rather than a globally optimized value. At higher pulse energies within the investigated range, the central laser-modified track becomes more pronounced, while guiding remains stress-assisted and spatially displaced from the directly modified region. Pulse energies beyond the investigated process window were not systematically studied, but further increases are expected to eventually promote stronger material damage, scattering, or substrate defects rather than continued improvement of the guided mode.

The BF33 writing regime offers two practical advantages for the proof-of-principle devices demonstrated in this work. First, the mode-field diameter remains comparatively stable within the tested pulse energy interval, which is important for the fabrication of directional couplers and Mach–Zehnder interferometers. Second, single-scan writing at 30 mm/s substantially reduces fabrication time compared with multiscan waveguide writing. As a result, test circuits containing waveguides, directional couplers, and interferometers could be fabricated within minutes rather than hours, which facilitates rapid design iteration and process optimization.

To estimate optical propagation losses, waveguides with lengths between 0.7 cm and 3.5 cm were characterized using the cut-back method. The measured insertion loss was plotted as a function of waveguide length and fitted using a linear model. From this fit, a propagation loss of approximately 0.3 dB/cm was obtained (Figure 8). This value remains above the lowest losses reported for optimized fused silica multiscan waveguides, but it is suitable for the interferometric proof-of-principle devices demonstrated in this work. The extracted coupling loss should be interpreted with caution, since it includes contributions from facet quality, mode mismatch, Fresnel reflections, and alignment uncertainty.

The influence of waveguide curvature was investigated for bend radii between 5 mm and 60 mm. As expected, transmission decreased for smaller bend radii due to bend-induced radiation losses and possible mode deformation. For bend radii above approximately 40 mm, the transmission approached a plateau within the measurement uncertainty, indicating that additional bend loss became small compared with the other loss contributions for the geometries used in this study.

Overall, these results show that BF33 supports fast single-scan fabrication of stress-assisted waveguides with mode-field properties and losses suitable for the interferometric circuits investigated here. The main advantage of the material platform developed in this work is not record-low propagation loss, but the combination of practical optical performance, high writing speed, and compatibility with the subsequent FLICE-based microstructuring steps.

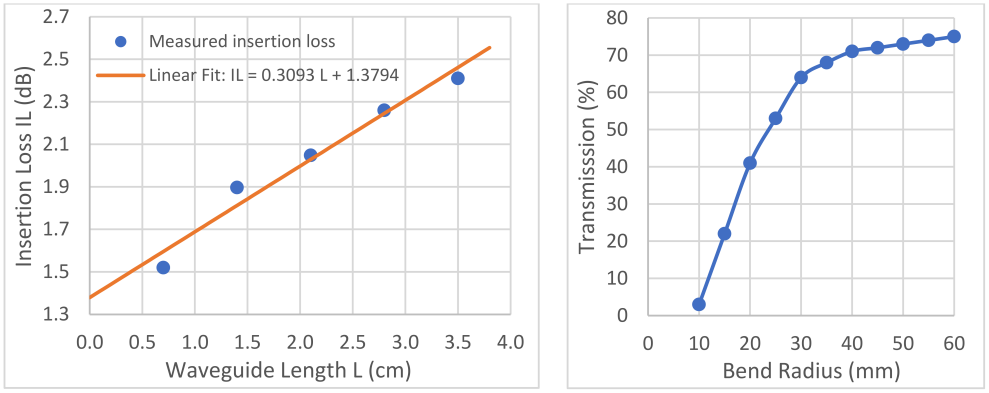


**Figure 8.** Optical loss characterization of stress-assisted waveguides in BF33 borosilicate glass. (**Left**) insertion loss as a function of waveguide length measured using the cut-back method at 808 nm. The solid line represents a linear fit; its slope was used to estimate the propagation loss. The fit intercept contains length-independent loss contributions, including input/output coupling losses, Fresnel reflections, facet quality, mode mismatch, and alignment uncertainty, and should therefore not be interpreted as a pure coupling loss. (**Right**) measured transmission as a function of bend radius for waveguides fabricated with the selected BF33 writing parameters.

**Evanescent Field Directional Couplers:** Directional couplers are essential building blocks of Mach–Zehnder interferometers and larger interferometric photonic circuits. To identify suitable coupler geometries for the BF33 platform, the coupling behavior was investigated as a function of the waveguide separation in the interaction region.

Directional couplers with an interaction length of 300 µm were fabricated in BF33 glass. This relatively short interaction length was chosen to limit the footprint of the Mach–Zehnder interferometers. The coupling distance was varied from 4.0 µm to 10.0 µm in increments of 0.2 µm, while all other fabrication parameters were kept constant. The waveguides were written at a depth of 200 µm using the optimized stress-assisted BF33 writing parameters. A bend radius of 50 mm was chosen to reduce bend-induced losses in the approach and separation regions.

Figure 9 (left part) shows the normalized output power measured at the bar and cross-ports as a function of waveguide separation in the coupling region. Increasing waveguide separation reduces the coupling strength, causing periodic power transfer between the waveguides and therefore periodic changes in the output splitting ratio. For the chosen interaction length, near-50:50 splitting was observed at coupling distances of approximately 4.1 µm, 5.5 µm, and 8.5 µm. The largest distance (8.5 µm), which is approximately equal to the mode-field diameter, was selected for subsequent MZI fabrication. Beyond this separation, the coupling strength decreases monotonically and no further 50:50 operating point is expected for the fixed interaction length. The larger spacing also minimizes interactions between neighboring laser-modified regions during writing, thereby improving fabrication robustness.

The polarization response of a nominally balanced coupler fabricated with the selected coupling distance was also evaluated. For the tested input polarization states, the measured bar-port transmission showed no systematic variation exceeding the experimental uncertainty. This indicates that the selected coupler geometry is sufficiently insensitive to the input polarization states for the interferometric measurements reported here. A more comprehensive polarization characterization, including arbitrary input states and both output ports, was not performed in this study.

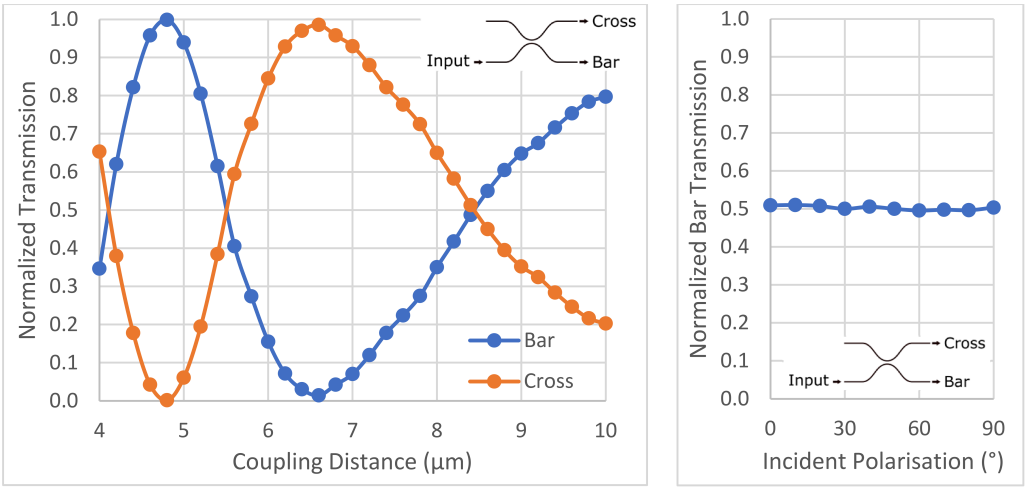


**Figure 9.** Directional coupler characterization in BF33. (**Left**) normalized output power measured at the bar and cross-ports as a function of waveguide separation in the coupling region for directional couplers with an interaction length of 300 µm at 808 nm. The bar and cross-signals are normalized output-port powers used to evaluate the splitting behavior; they should not be interpreted as independently calibrated absolute transmission values whose sum is required to be exactly unity. (**Right**) measured bar-port transmission of a nominally balanced directional coupler as a function of the tested input polarization state.

**Device-to-Device Consistency of Waveguides, Directional Couplers, and Interferometers:** To assess device-to-device consistency within a single fabrication run, a test chip containing ten nominally identical straight waveguides, directional couplers, Mach–Zehnder interferometers, and cascaded double-MZI structures was fabricated. Before fabricating the test chip, a calibration series of directional couplers with varying coupling distances was written to determine the coupling distance required for an approximately balanced splitting ratio under the current writing conditions. This calibration was repeated before each fabrication run of interferometric structures to account for day-to-day variations in the laser-writing system, such as small changes in laser power, beam alignment, or focusing conditions. The calibrated coupling distance was then used for the interferometric structures on the corresponding chip.

The ten straight waveguides exhibited consistent optical behavior. The measured transmission was 73 $\pm$ 3.6%, and the mode-field diameters were 7.78 $\pm$ 0.04 µm and 8.82 $\pm$ 0.04 µm along the two principal axes. These values include contributions from measurement uncertainty, alignment repeatability, and facet quality. They should therefore be interpreted as an estimate of the combined variation in fabrication and characterization, rather than as a pure process-variation metric.

The directional couplers fabricated on the same chip showed limited variation in splitting behavior. Given the strong dependence of evanescent coupling on waveguide separation, this result indicates that the selected BF33 writing process provides sufficient geometrical consistency for the fabrication of the MZI structures investigated in this work.

The Mach–Zehnder interferometers and cascaded double-MZI structures were used to test whether the calibrated directional couplers could be combined into functional interferometric circuits. In an ideal balanced MZI composed of two identical 50:50 directional couplers, the characteristic $\pi/2$ phase shift associated with directional coupling results in complete power transfer to the cross-port. Cascading two such MZI stages reverses this routing behavior, resulting in complete power transfer back to the bar port. In practice, deviations from ideal 50:50 coupling, fabrication asymmetries, and propagation–loss imbalance can reduce the achievable routing contrast. The device-to-device consistency of the

directional couplers, single MZIs, and cascaded double-MZI structures is summarized in Figure 10.

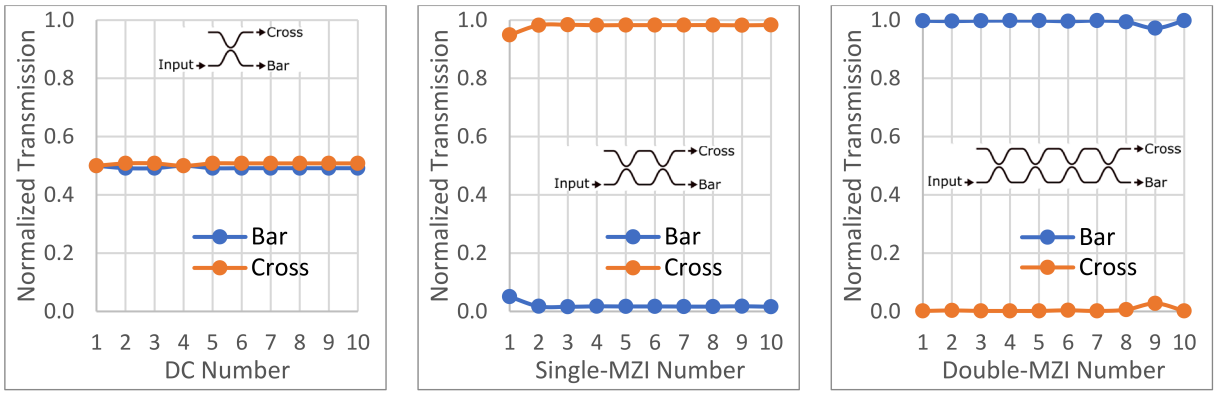


**Figure 10.** Device-to-device consistency of interferometric building blocks fabricated in BF33. Results are shown for ten nominally identical directional couplers, Mach–Zehnder interferometers, and cascaded double-MZI structures fabricated on the same test chip.

The measured single-MZIs and cascaded double-MZI structures displayed the expected routing behavior within the experimental uncertainty. The single-MZIs predominantly routed light to the cross-port, while the cascaded double-MZI structures predominantly routed light back to the bar port. These measurements confirm that the fabricated waveguides and directional couplers can be combined into functional interferometric circuits. At the level of the two-stage cascaded structures tested here, no clear degradation of the intended routing behavior was observed.

These results indicate good device-to-device consistency within a single fabrication run. They do not, however, constitute a comprehensive statistical process analysis. Further studies involving multiple chips, repeated fabrication runs, yield analysis, long-term stability measurements, and larger interferometric networks would be required to quantify process reproducibility and scalability in detail.

**FLICE-Fabricated Suspended Microbridges for Thermo-Optic Phase Shifters:** A central objective of this work was to integrate thermo-optic phase shifters into femtosecond-laser-written interferometric circuits using FLICE-fabricated suspended microbridges. The intended function of the suspended geometry is to thermally isolate the heated waveguide section from the surrounding substrate, thereby reducing the electrical power required for phase tuning and minimizing thermal crosstalk. In this study, the focus was on demonstrating the fabrication and operation of such integrated structures, while quantitative thermal crosstalk measurements were not performed.

Figure 11 shows a representative suspended microbridge fabricated by FLICE. Microbridges with different lengths were fabricated during process development. The SEM image depicts a 1.5 mm long microbridge with a cross-section of approximately 60 µm × 60 µm. The thermo-optic characterization presented in this work was performed using a 3 mm long microbridge of the same cross-section. A femtosecond-laser-written waveguide passes through the center of the bridge, while the Cr/Au metallization layer deposited on the chip surface also covers the microbridge and forms the resistive heater. Tapered support regions provide mechanical stability and connect the suspended section to the surrounding substrate and surface contact pads.

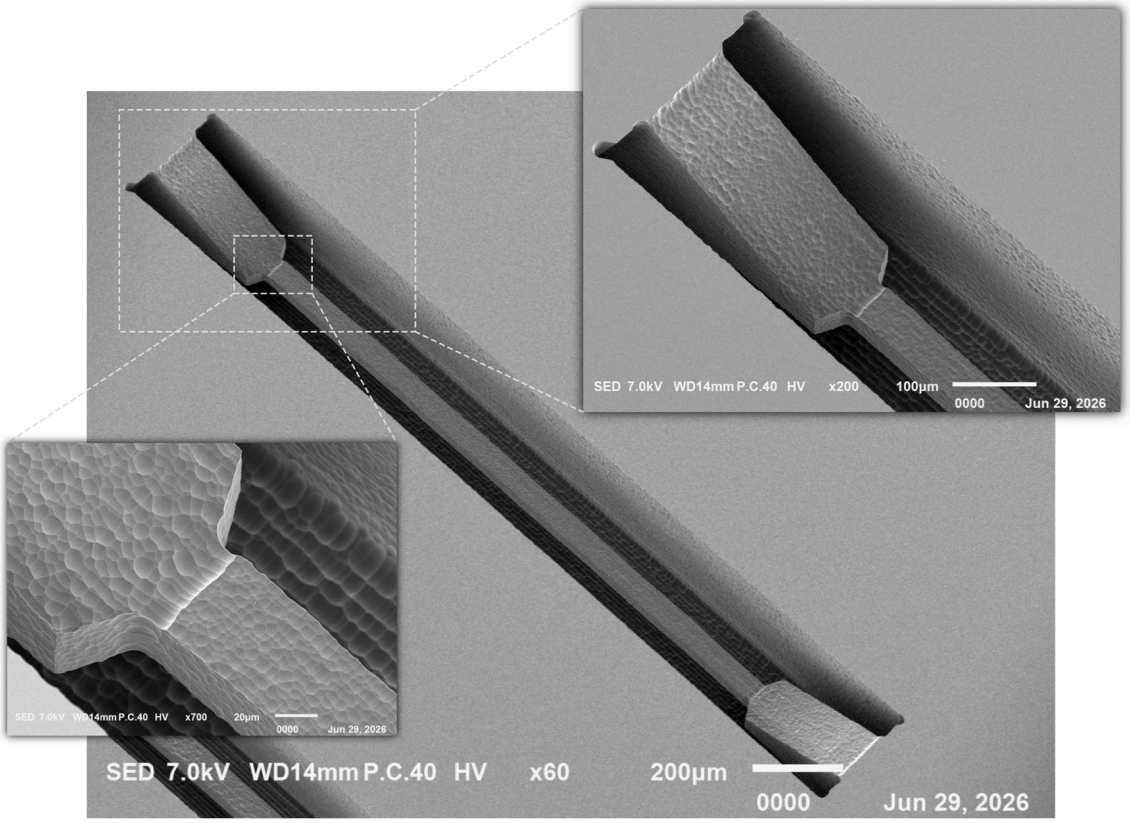


**Figure 11.** Scanning electron micrograph of a representative FLICE-fabricated suspended microbridge with a length of 1.5 mm and a nominal cross-section of approximately 60 µm × 60 µm. The thermo-optic characterization was performed on a 3 mm-long microbridge with the same nominal cross-section. The etched cavity provides thermal isolation of the bridge region, while tapered support structures ensure mechanical attachment to the surrounding substrate and electrical connection to the surface contact pads. The insets show higher-magnification views of the tapered support region, illustrating the quality of the FLICE-fabricated surfaces and the structural fidelity of the fabricated geometry.

The microbridge structures were generated from a parametric CAD model, which allows the bridge length, width, height, waveguide position, and air-gap geometry to be adjusted. To reduce laser writing time during FLICE exposure, the volume to be removed was divided into detachable sub-volumes. Instead of exposing the complete volume, only selected boundary surfaces and separator structures were written. During wet-chemical etching, these exposed regions promoted separation and removal of the sacrificial glass fragments. The fabricated microbridges reproduced the intended overall geometry and remained mechanically stable after etching, metallization, and chip handling.

The alignment between previously written waveguides and subsequently fabricated microbridges was evaluated using test structures with deliberately varied nominal offsets. Figure 12 shows a facet-view micrograph of such FLICE structures prior to chemical etching. The structure with zero nominal offset showed the best overlap between the waveguide and the microbridge center, confirming that the alignment-mark-based registration procedure was sufficient for the integrated devices demonstrated in this work.

The results demonstrate that the FLICE process can be registered to previously written waveguides and used to release suspended bridge structures within the same borosilicate-glass substrate. However, the present study did not include a systematic statistical analysis of dimensional tolerances, surface roughness, yield, or mechanical reliability across a large number of devices.

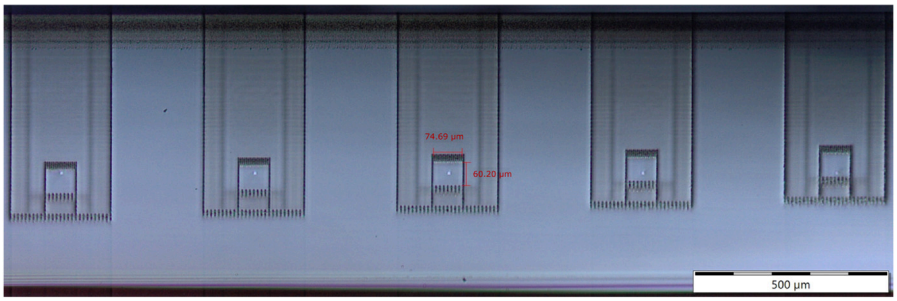


**Figure 12.** Facet-view optical transmission micrograph of test structures comprising femtosecond-laser-written waveguides and FLICE-defined microbridge geometries in fused silica prior to chemical etching. The samples were cleaved to expose the cross-section and imaged under transmitted-light illumination. The bright feature corresponds to the optical waveguide, whereas the dark square represents the microbridge cross-section. Five structures with nominal relative offsets of −20, −10, 0, +10, and +20 µm are shown. The same alignment strategy was applied to BF33, where comparable registration accuracy was achieved.

For the suspended microbridge structures used in the thermo-optic devices, FLICE writing was performed using a pulse energy of approximately 500 nJ, a pulse duration of 2.5 ps, and hatching/slicing distances between 2 µm and 6 µm. After selective etching in KOH, mechanically stable suspended microbridges were obtained. Together with the alignment tests, these results show that FLICE can be combined with stress-assisted BF33 waveguides to fabricate suspended structures positioned around selected waveguide sections.

**Thermo-Optic Tuning of Suspended Microbridge Mach–Zehnder Interferometers:** After completion of waveguide writing, FLICE processing, facet preparation, Cr/Au metallization, laser patterning of the electrical contacts, and PCB mounting, the suspended microbridge phase shifter was characterized within Mach–Zehnder interferometers. The phase shifter was positioned on one arm of the MZI, allowing the optical phase in that arm to be tuned by electrical heating.

Figure 13 shows the optical transmission at the bar and cross-ports as a function of the electrical power dissipated in the heater. The two outputs exhibit complementary modulation, confirming thermo-optic phase tuning of the interferometer. From one full period of the transmission response, the electrical power required for a full $2\pi$ phase shift was determined to be approximately 17 mW. This value indicates efficient thermo-optic tuning for the suspended microbridge geometry and is consistent with thermal isolation of the heated waveguide section from the surrounding glass substrate. The absolute output transmission of the thermo-optic MZI is lower than that of the straight waveguides used for the propagation–loss characterization because the MZI contains additional loss contributions from two directional couplers, curved waveguide sections, the suspended microbridge region, bridge transitions, metallization and patterning steps, as well as coupling and facet variations. Therefore, the summed bar and cross-port transmission in Figure 13 should not be directly compared with the straight waveguide transmission in Figure 8.

The temporal response of the phase shifter inside the MZI was evaluated by switching the heater power between values corresponding approximately to transmission minima and maxima. The measured rise and fall times of the modulated optical signal were on the order of 100 ms. This response time reflects the expected trade-off between thermal isolation and switching speed in suspended thermo-optic structures: stronger thermal isolation can reduce the required tuning power, but it also reduces heat dissipation and can therefore increase the thermal time constant.

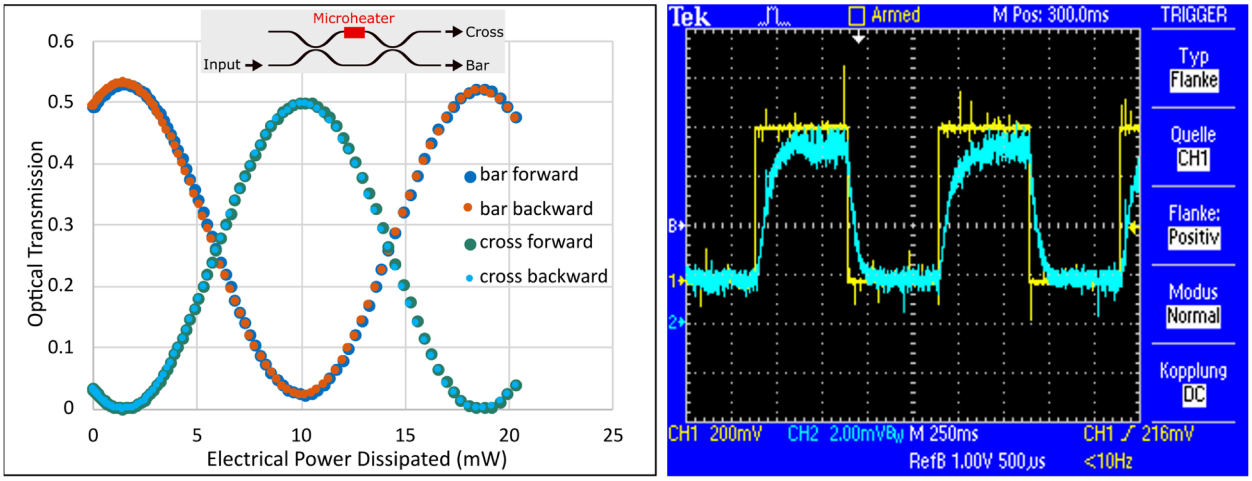


**Figure 13.** Thermo-optic characterization of a Mach–Zehnder interferometer incorporating a FLICE-fabricated suspended microbridge phase shifter. (**Left**) measured output transmission at the bar and cross-ports as a function of applied electrical power at 808 nm. "Forward" and "backward" denote increasing and decreasing voltage sweeps, respectively. The inset schematically illustrates the MZI with the integrated microheater located on one interferometer arm. (**Right**) temporal response of the interferometer during electrical heater modulation. The yellow trace shows the voltage applied to the resistive heater, while the light-blue trace shows the optical signal recorded at one output port of the Mach–Zehnder interferometer.

The demonstrated 2π tuning power of approximately 17 mW is the most direct quantitative performance metric of the suspended microbridge phase shifter. It confirms active reconfiguration of a femtosecond-laser-written BF33 Mach–Zehnder interferometer using a FLICE-fabricated suspended structure with an integrated resistive heater. Since thermal crosstalk between neighboring phase shifters was not measured in this study, the suspended microbridge is presented as a FLICE-based concept for thermally isolated phase-shifter integration rather than a quantitatively verified low-crosstalk architecture.

To provide an overview of the fabricated device and its experimental context, Figure 14 shows the optical chip mounted on a custom printed circuit board in the measurement station. The photograph illustrates the end-fire coupling and optical readout configuration, including the input objective for coupling light into the laser-written waveguides and the output-side imaging optics used to image the waveguide outputs onto a CMOS sensor. Since the laser-written waveguides and FLICE-defined structures are not fully visible in the overview photograph, the figure also includes insets showing a schematic representation of the relevant internal layout as well as a transmitted light micrograph of part of a suspended microbridge with its corresponding MZI waveguides.

Together, the results demonstrate the feasibility of combining stress-assisted femtosecond-laser-written waveguides, directional couplers, Mach–Zehnder interferometers, FLICE-fabricated suspended microbridges, and resistive microheaters within a single borosilicate glass substrate. The demonstrated devices validate the basic fabrication concept and the thermo-optic functionality of the integrated phase shifters. Future work should address statistical process characterization, dimensional tolerances of the FLICE structures, heater lifetime, thermal crosstalk in dense layouts, and scaling toward larger programmable photonic circuits.

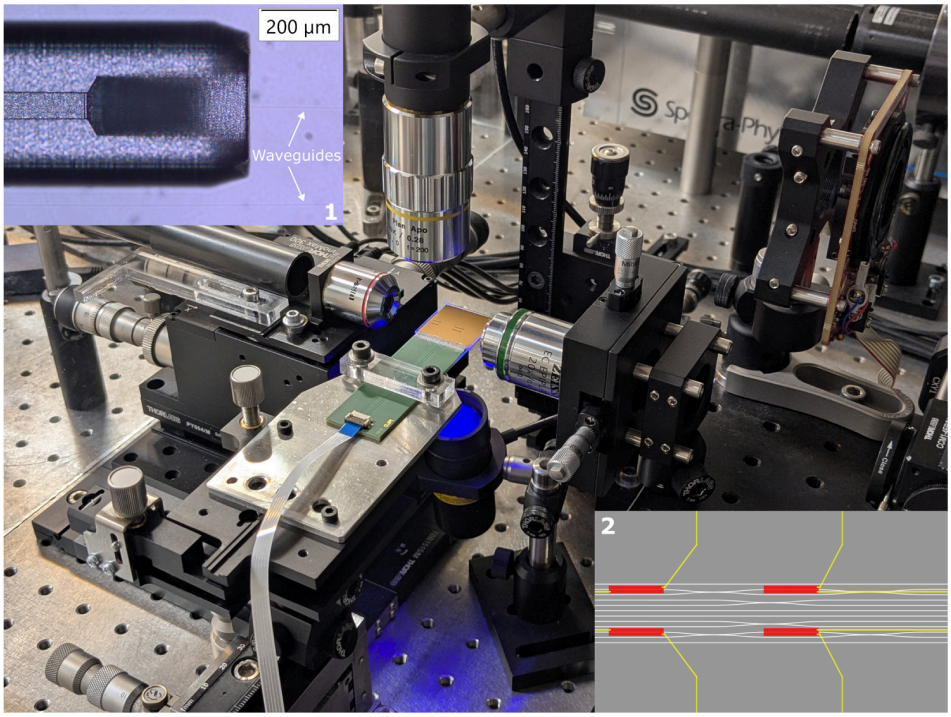


**Figure 14.** Overview photograph of the fabricated optical chip mounted on a custom printed circuit board in the measurement station, corresponding to the setup schematically shown in Figure 5. The PCB provides five electrical contact pads, four connected to individual microheaters and one central ground pad; electrical contact to the chip was established using conductive adhesive with the metallized surface of the chip being placed face down onto the PCB. Additional structural adhesive along the lateral chip edges provides mechanical stabilization. Inset (**1**): transmitted-light micrograph of a representative chip before metallization, showing part of a suspended microbridge with its corresponding MZI waveguides. The laser-written waveguides are only weakly visible in transmitted-light microscopy because it produces primarily a phase-contrast signal. Inset (**2**): schematic representation of the relevant device layout. Waveguides are shown in white, FLICE phase-shifter trajectories in red, and ablation lines for contact pads in yellow. The layout contains two Mach–Zehnder interferometers with thermo-optic phase shifters and nominal 50:50 directional couplers. The two outer channels are used for fiber-array alignment, while the ten central channels have a pitch of 250 µm and are compatible with fiber-array coupling. Thermo-optic phase tuning was performed using only the central microheaters.

## 4. Discussion

In this work, we demonstrated a monolithic fabrication route for reconfigurable three-dimensional photonic circuits in borosilicate glass by combining femtosecond laser writing (FLW) and femtosecond laser-induced chemical etching (FLICE). The most important outcome is the experimental validation of a process chain in which FLW provides three-dimensional waveguide circuits, while FLICE adds suspended microstructures that can be aligned to previously written waveguides within the same substrate. In the devices studied here, this combination enabled suspended thermo-optic phase shifters integrated into Mach–Zehnder interferometers and yielded a full $2\pi$ phase shift with an electrical power of approximately 17 mW. Together, these results validate the basic concept of monolithically integrated reconfigurable photonic building blocks in BF33.

The present devices were characterized using classical continuous-wave light and do not demonstrate quantum-optical operation, single-photon interference, or multiphoton functionality. Their relevance to future quantum photonic circuits lies in the demonstrated implementation of linear optical building blocks—waveguides, directional couplers, Mach–Zehnder interferometers, and thermo-optic phase shifters—that are also required in

programmable quantum photonic processors. Future use in quantum photonic applications will require additional characterization of single-photon compatibility, propagation-loss budget, phase stability, coupler uniformity, thermal crosstalk, calibration stability, and compatibility with the wavelengths of the intended photon sources and detectors.

A second key result is the identification of a practically useful stress-assisted waveguide writing regime in BF33. In contrast to multiscan waveguides in fused silica, the BF33 approach relies on single-scan writing at 30 mm/s, substantially reducing fabrication time while still providing optical guiding, directional coupling, and interferometric operation with sufficient consistency for proof-of-principle circuits. The main advantage of this platform is therefore not record-low propagation loss, but the combination of fast waveguide fabrication, a comparatively robust writing window, and compatibility with FLICE-based microstructuring.

Previous FLW-based reconfigurable photonic circuits have demonstrated thermo-optic tuning and reduced crosstalk using surface heaters and thermal-isolation strategies in glass platforms [10]. In contrast, the present approach uses FLICE to define a suspended waveguide-carrying microbridge that also carries the resistive heater, thereby integrating optical, mechanical, and electrical functionality within a monolithic borosilicate glass chip.

At the same time, the present results should be interpreted as a building-block-level validation rather than as a full demonstration of scalable programmable photonic circuits. During the voltage sweeps used for the thermo-optic characterization, no qualitative evidence of irreversible device degradation or pronounced hysteresis was observed. However, dedicated measurements of hysteresis, long-term drift, electrical cycling stability, and thermal crosstalk between neighboring phase shifters were not performed and remain important next steps. Furthermore, this study did not yet include a comprehensive statistical analysis across multiple fabrication runs, a quantitative evaluation of thermal crosstalk in dense layouts, or long-term heater reliability testing. Likewise, larger-scale implementations will require further study of propagation–loss accumulation, coupler uniformity, phase stability, electrical routing, packaging, and calibration strategies. The suspended microbridge should therefore be regarded as a demonstrated thermo-optic integration concept, but not yet as a fully characterized low-crosstalk architecture.

From a fabrication perspective, waveguide writing accounted for only a minor fraction of the total laser-processing time in the demonstrated devices, whereas FLICE exposure of the suspended microbridge structures dominated the workflow. Under the present process conditions, a typical 3 mm long suspended heater structure required about 20 min of FLICE writing time, which is well suited for laboratory-scale prototyping and small-batch fabrication. Future work should therefore focus not only on device-level optimization, but also on shortening FLICE exposure times through faster scanning strategies, improved sacrificial volume design, and optimized etchant access. In addition, systematic variations in bridge geometry, heater layout, and support design will be important for balancing tuning power, response speed, mechanical robustness, and thermal interaction with neighboring components.

FLICE also offers a broader three-dimensional design space beyond the suspended thermo-optic phase shifter demonstrated here. Because it enables free-form buried microstructures in glass, it may support future active and passive device concepts that combine waveguides with mechanically compliant elements, cavities, channels, or hybrid photonic-mechanical structures. In the context of the present work, however, this broader perspective should be understood as an outlook rather than as an experimentally established result.

## 5. Conclusions

In conclusion, the combination of FLW and FLICE provides a versatile route for integrating laser-written photonic circuits with three-dimensionally defined functional

microstructures in glass. The demonstrated integration of stress-assisted waveguides, directional couplers, Mach–Zehnder interferometers, suspended FLICE microbridges, and resistive microheaters establishes the feasibility of monolithic thermo-optically reconfigurable photonic circuits in borosilicate glass. The work provides a strong proof-of-principle basis for future programmable glass photonic systems. The next steps are a systematic quantification of inter-run reproducibility, propagation-loss accumulation, thermal crosstalk, long-term heater stability, and circuit-level scalability in larger interferometric networks.

**Author Contributions:** Conceptualization, B.L.; methodology, B.L. and G.S.; software, G.S.; validation, P.L., P.H. and B.L.; formal analysis, P.L., P.H. and B.L.; investigation, P.L., P.H. and B.L.; resources, B.L.; writing—original draft preparation, B.L.; writing—review and editing, P.L., P.H., G.S. and B.L.; visualization, B.L., P.H. and P.L.; supervision, B.L.; project administration, B.L.; funding acquisition, B.L. All authors have read and agreed to the published version of the manuscript.

**Funding:** This research was funded by the Austrian Research Promotion Agency (FFG), primarily through the projects FLMOptChips (grant no. 45020820) and PIQLearn (grant no. 54993960). Foundational developments underlying the presented work were carried out within the FFG project OptoQuant (grant no. 37798980). Additional support was provided through the FFG project ScaleQUDITS (grant no. 55140015).

**Institutional Review Board Statement:** Not applicable.

**Informed Consent Statement:** Not applicable.

**Data Availability Statement:** The data presented in this study are available from the corresponding author upon reasonable request.

**Acknowledgments:** The authors thank Georg Jakopic (JOANNEUM RESEARCH) for his encouragement, continued interest in this work, valuable support throughout the project, and assistance in navigating the often time-consuming administrative and funding-related processes associated with collaborative research projects. During the preparation of this manuscript, the authors used OpenAI ChatGPT (GPT-5) for language editing, text refinement, and preparation of a schematic illustration (Figure 4). The authors reviewed and edited all generated content and take full responsibility for the content of this publication.

**Conflicts of Interest:** The authors declare no conflicts of interest. The funders had no role in the design of the study; in the collection, analyses, or interpretation of data; in the writing of the manuscript; or in the decision to publish the results.

## Abbreviations

The following abbreviations are used in this manuscript:

| | |
|---|---|
| BF33 | SCHOTT BOROFLOAT® 33 |
| CAD | Computer-Aided Design |
| Cr/Au | Chromium/Gold |
| FLICE | Femtosecond Laser-Induced Chemical Etching |
| FLM | Femtosecond Laser Micromachining |
| MFD | Mode-Field Diameter |
| FLW | Femtosecond Laser Writing |
| MZI | Mach–Zehnder Interferometer |
| NA | Numerical Aperture |
| KOH | Potassium Hydroxide |
| PCB | Printed Circuit Board |
| FS | Fused Silica |
| SEM | Scanning Electron Microscope |

## References


1. Politi, A.; Cryan, M.J.; Rarity, J.G.; Yu, S.; O'Brien, J.L. Silica-on-Silicon Waveguide Quantum Circuits. *Science* **2008**, *320*, 646–649. [CrossRef] [PubMed]
2. Matthews, J.C.F.; Politi, A.; Stefanov, A.; O'Brien, J.L. Manipulation of Multiphoton Entanglement in Waveguide Quantum Circuits. *Nat. Photon* **2009**, *3*, 346–350. [CrossRef]
3. Miller, D.A.B. Self-Configuring Universal Linear Optical Component [Invited]. *Photon. Res.* **2013**, *1*, 1–15. [CrossRef]
4. Carolan, J.; Harrold, C.; Sparrow, C.; Martín-López, E.; Russell, N.J.; Silverstone, J.W.; Shadbolt, P.J.; Matsuda, N.; Oguma, M.; Itoh, M.; et al. Universal Linear Optics. *Science* **2015**, *349*, 711–716. [CrossRef] [PubMed]
5. Reck, M.; Zeilinger, A.; Bernstein, H.J.; Bertani, P. Experimental Realization of Any Discrete Unitary Operator. *Phys. Rev. Lett.* **1994**, *73*, 58–61. [CrossRef] [PubMed]
6. Clements, W.R.; Humphreys, P.C.; Metcalf, B.J.; Kolthammer, W.S.; Walsmley, I.A. Optimal Design for Universal Multiport Interferometers. *Optica* **2016**, *3*, 1460. [CrossRef]
7. Harris, N.C.; Ma, Y.; Mower, J.; Baehr-Jones, T.; Englund, D.; Hochberg, M.; Galland, C. Efficient, Compact and Low Loss Thermo-Optic Phase Shifter in Silicon. *Opt. Express* **2014**, *22*, 10487. [CrossRef] [PubMed]
8. Flamini, F.; Magrini, L.; Rab, A.S.; Spagnolo, N.; D'Ambrosio, V.; Mataloni, P.; Sciarrino, F.; Zandrini, T.; Crespi, A.; Ramponi, R.; et al. Thermally Reconfigurable Quantum Photonic Circuits at Telecom Wavelength by Femtosecond Laser Micromachining. *Light. Sci. Appl.* **2015**, *4*, e354. [CrossRef]
9. Ceccarelli, F.; Atzeni, S.; Prencipe, A.; Farinaro, R.; Osellame, R. Thermal Phase Shifters for Femtosecond Laser Written Photonic Integrated Circuits. *J. Light. Technol.* **2019**, *37*, 4275–4281. [CrossRef]
10. Ceccarelli, F.; Atzeni, S.; Pentangelo, C.; Pellegatta, F.; Crespi, A.; Osellame, R. Low Power Reconfigurability and Reduced Crosstalk in Integrated Photonic Circuits Fabricated by Femtosecond Laser Micromachining. *Laser Photonics Rev.* **2020**, *14*, 2000024. [CrossRef]
11. Calvarese, M.; Paiè, P.; Ceccarelli, F.; Sala, F.; Bassi, A.; Osellame, R.; Bragheri, F. Strategies for Improved Temporal Response of Glass-Based Optical Switches. *Sci. Rep.* **2022**, *12*, 239. [CrossRef] [PubMed]
12. Davis, K.M.; Miura, K.; Sugimoto, N.; Hirao, K. Writing Waveguides in Glass with a Femtosecond Laser. *Opt. Lett.* **1996**, *21*, 1729. [CrossRef] [PubMed]
13. Will, M.; Nolte, S.; Chichkov, B.N.; Tünnermann, A. Optical Properties of Waveguides Fabricated in Fused Silica by Femtosecond Laser Pulses. *Appl. Opt.* **2002**, *41*, 4360. [CrossRef] [PubMed]
14. Gattass, R.R.; Mazur, E. Femtosecond Laser Micromachining in Transparent Materials. *Nat. Photon* **2008**, *2*, 219–225. [CrossRef]
15. Osellame, R.; Cerullo, G.; Ramponi, R. (Eds.) *Femtosecond Laser Micromachining: Photonic and Microfluidic Devices in Transparent Materials*; Topics in Applied Physics; Springer: Berlin/Heidelberg, Germany, 2012; Volume 123, ISBN 978-3-642-23365-4.
16. Spagnolo, N.; Vitelli, C.; Aparo, L.; Mataloni, P.; Sciarrino, F.; Crespi, A.; Ramponi, R.; Osellame, R. Three-Photon Bosonic Coalescence in an Integrated Tritter. *Nat. Commun.* **2013**, *4*, 1606. [CrossRef] [PubMed]
17. Caruso, F.; Crespi, A.; Ciriolo, A.G.; Sciarrino, F.; Osellame, R. Fast Escape of a Quantum Walker from an Integrated Photonic Maze. *Nat. Commun.* **2016**, *7*, 11682. [CrossRef] [PubMed]
18. Corrielli, G.; Crespi, A.; Osellame, R. Femtosecond Laser Micromachining for Integrated Quantum Photonics. *Nanophotonics* **2021**, *10*, 3789–3812. [CrossRef]
19. Skryabin, N.N.; Zhuravitskii, S.A.; Dyakonov, I.V.; Straupe, S.S.; Kalinkin, A.A.; Kulik, S.P. Femtosecond-Laser-Written Low-Loss Multiscan Waveguides in Fused Silica. *Phys. Rev. Appl.* **2024**, *22*, 064079. [CrossRef]
20. Barzaghi, A.; Bénéfice, M.; Ceccarelli, F.; Corrielli, G.; Galli, V.; Gardina, M.; Grimaldi, V.; Kaczorowski, J.; Malaspina, F.; Osellame, R.; et al. A 24-Mode Laser-Written Universal Photonic Processor in a Glass-Based Platform. In Proceedings of the Volume 13391 of SPIE Quantum West, San Francisco, CA, USA, 25–31 January 2025; Article 1339112. [CrossRef]
21. Albiero, R.; Pentangelo, C.; Gardina, M.; Atzeni, S.; Ceccarelli, F.; Osellame, R. Toward Higher Integration Density in Femtosecond-Laser-Written Programmable Photonic Circuits. *Micromachines* **2022**, *13*, 1145. [CrossRef] [PubMed]
22. Pentangelo, C.; Giano, N.D.; Piacentini, S.; Arpe, R.; Ceccarelli, F.; Crespi, A.; Osellame, R. High-Fidelity and Polarization Insensitive Universal Photonic Processors Fabricated by Femtosecond Laser Writing. *Nanophotonics* **2024**, *13*, 2259–2270. [CrossRef] [PubMed]
23. Kondratyev, I.V.; Urusova, K.N.; Argenchiev, A.S.; Klushnikov, N.S.; Kuzmin, S.S.; Skryabin, N.N.; Golikov, A.D.; Kovalyuk, V.V.; Goltsman, G.N.; Dyakonov, I.V.; et al. Effective Programming of a Photonic Processor with Complex Interferometric Structure 2025. *Phys. Rev. Appl.* **2026**, *25*, 034072. [CrossRef]
24. Gottmann, J.; Hermans, M.; Repiev, N.; Ortmann, J. Selective Laser-Induced Etching of 3D Precision Quartz Glass Components for Microfluidic Applications—Up-Scaling of Complexity and Speed. *Micromachines* **2017**, *8*, 110. [CrossRef]
25. Butkutė, A.; Merkininkaitė, G.; Jurkšas, T.; Stančikas, J.; Baravykas, T.; Vargalis, R.; Tičkūnas, T.; Bachmann, J.; Šakirzanovas, S.; Sirutkaitis, V.; et al. Femtosecond Laser Assisted 3D Etching Using Inorganic-Organic Etchant. *Materials* **2022**, *15*, 2817. [CrossRef] [PubMed]

26. Bischof, D.; Kahl, M.; Michler, M. Laser-Assisted Etching of Borosilicate Glass in Potassium Hydroxide. *Opt. Mater. Express* **2021**, *11*, 1185. [CrossRef]
27. Vazquez, R.M.; Osellame, R.; Nolli, D.; Dongre, C.; Van Den Vlekkert, H.; Ramponi, R.; Pollnau, M.; Cerullo, G. Integration of Femtosecond Laser Written Optical Waveguides in a Lab-on-Chip. *Lab. Chip* **2009**, *9*, 91–96. [CrossRef] [PubMed]
28. Crespi, A.; Gu, Y.; Ngamsom, B.; Hoekstra, H.J.W.M.; Dongre, C.; Pollnau, M.; Ramponi, R.; Van Den Vlekkert, H.H.; Watts, P.; Cerullo, G.; et al. Three-Dimensional Mach-Zehnder Interferometer in a Microfluidic Chip for Spatially-Resolved Label-Free Detection. *Lab. Chip* **2010**, *10*, 1167. [CrossRef] [PubMed]
29. Maia, J.M.; Amorim, V.A.; Viveiros, D.; Marques, P.V.S. Femtosecond Laser Micromachining of an Optofluidics-Based Monolithic Whispering-Gallery Mode Resonator Coupled to a Suspended Waveguide. *Sci. Rep.* **2021**, *11*, 9128. [CrossRef] [PubMed]
30. Piacentini, S.; Bragheri, F.; Corrielli, G.; Martínez Vázquez, R.; Paiè, P.; Osellame, R. Advanced Photonic and Optofluidic Devices Fabricated in Glass via Femtosecond Laser Micromachining [Invited]. *Opt. Mater. Express* **2022**, *12*, 3930. [CrossRef]
31. Tan, D.; Sun, X.; Wang, Q.; Zhou, P.; Liao, Y.; Qiu, J. Fabricating Low Loss Waveguides over a Large Depth in Glass by Temperature Gradient Assisted Femtosecond Laser Writing. *Opt. Lett.* **2020**, *45*, 3941. [CrossRef] [PubMed]
32. Babu, B.H.; Niu, M.; Billotte, T.; Bi, P.; Zheng, F.; Poumellec, B.; Lancry, M.; Hao, X.-T. Femtosecond Laser Processing Induced Low Loss Waveguides in Multicomponent Glasses. *Opt. Mater. Express* **2017**, *7*, 3580. [CrossRef]


**Disclaimer/Publisher's Note:** The statements, opinions and data contained in all publications are solely those of the individual author(s) and contributor(s) and not of MDPI and/or the editor(s). MDPI and/or the editor(s) disclaim responsibility for any injury to people or property resulting from any ideas, methods, instructions or products referred to in the content.